The Binding of Substrate Analogs to Phosphotriesterase*

Matthew M. Benning‡, Suk-Bong Hong§, Frank M. Raushel¶, and Hazel M. Holden‡∥

From the ‡Department of Biochemistry, University of Wisconsin, Madison, Wisconsin 53706, §Triad Therapeutics, San Diego, California 92121, and the ¶Department of Chemistry, Texas A&M University, College Station, Texas 77843

Phosphotriesterase (PTE) from *Pseudomonas diminuta* catalyzes the detoxification of organophosphates such as the widely utilized insecticide paraoxon and the chemical warfare agent sarin. The three-dimensional structure of the enzyme is known from high resolution x-ray crystallographic analyses. Each subunit of the homodimer folds into a so-called TIM barrel, with eight strands of parallel β-sheet. The two zinc ions required for activity are positioned at the C-terminal portion of the β-barrel. Here, we describe the three-dimensional structure of PTE complexed with the inhibitor diisopropyl methyl phosphonate, which serves as a mimic for sarin. Additionally, the structure of the enzyme complexed with triethyl phosphate is also presented. In the case of the PTE-diisopropyl methyl phosphonate complex, the phosphoryl oxygen of the inhibitor coordinates to the more solvent-exposed zinc ion (2.5 Å), thereby lending support to the presumed catalytic mechanism involving metal coordination of the substrate. In the PTE-triethyl phosphate complex, the phosphoryl oxygen of the inhibitor is positioned at 3.4 Å from the more solvent-exposed zinc ion. The two structures described in this report provide additional molecular understanding for the ability of this remarkable enzyme to hydrolyze such a wide range of organophosphorus substrates.

The bacterial enzyme phosphotriesterase (PTE)[1] catalyzes the hydrolysis of a wide range of organophosphate nerve agents, including the chemical warfare agents sarin, soman, and VX (1). The specific reaction catalyzed for the hydrolysis of the insecticide paraoxon is illustrated in Scheme 1. Measurements of the kinetic constants for this enzyme have demonstrated that the turnover numbers are remarkably high. For example, the k_{cat} and k_{cat}/K_m values for the hydrolysis of paraoxon approach 10^4 s^{-1} and 10^8 M^{-1} s^{-1}, respectively (2). Interestingly, a naturally occurring substrate has not, as yet, been identified. We have speculated that this catalytic activity recently evolved from a preexisting enzyme, due in part to the widespread use of high levels of organophosphate insecticides throughout the world (3).

The three-dimensional structure of PTE was solved several years ago by x-ray crystallographic analyses and an α-carbon trace of one subunit of the homodimer is displayed in Fig. 1 (4, 5). The protein folds into an $(\alpha\beta)_8$ motif that is very similar in size and shape to urease (6) and adenosine deaminase (7). The active site is located adjacent to a binuclear metal center located within the αβ-barrel. The native enzyme contains Zn^{2+}, but the two divalent cations can be substituted with Cd^{2+}, Co^{2+}, Ni^{2+}, or Mn^{2+} without loss of catalytic activity (2). The two metal ions are coordinated to the protein via complexation with four histidine residues (His-55, His-57, His-201, and His-230) and a single carboxylate from Asp-301 (5). In addition to these ligands, the two metal ions are bridged via a carboxylated lysine residue and a hydroxide from the solvent (5). The carboxylation of the ε-amino group of Lys-169 to form a carbamate functional group has also been observed in the structure of the related enzyme, urease (6). The bridging hydroxide is thought to be the nucleophile for the hydrolytic attack on the phosphorus center of the substrate.

The molecular structure of PTE has also been determined with the protein crystallized in the presence of a nonhydrolyzable inhibitor, diethyl 4-methylbenzyl phosphonate (Fig. 2, *compound I*) (8). The orientation of this inhibitor within the active site of PTE has defined the outlines of the binding pockets that accommodate the four substituents attached to the phosphorus core. In this structure, the *pro-S$_P$* ethoxy group of the inhibitor is pointed away from the binuclear metal center and toward the solvent. It is positioned within the active site in a manner expected of the leaving group prior to nucleophilic attack by the bridging hydroxide. The *pro-R$_P$* ethoxy group lies closest to the side chains of Ile-106, Leu-303, and Ser-308 (Fig. 1). The methylbenzyl substituent is pointed toward a pocket lined primarily with the side chains of His-257, Leu-271, and Met-317 (Fig. 1). Additionally, the phosphoryl oxygen of the inhibitor is located at 3.3 Å from the indole ring of Trp-131, 3.2 Å from the imidazole of His-201, and 3.5 Å from the more solvent-exposed divalent metal cation.
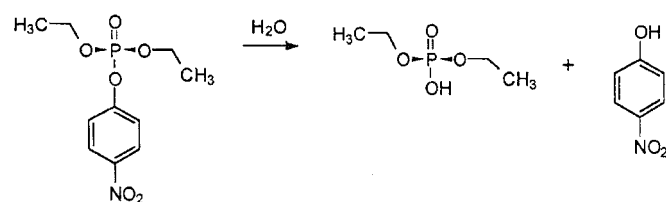
A recent investigation of the substrate and stereochemical specificity of PTE has demonstrated that the active site of this protein will accommodate a variety of substituents attached to the phosphorus center (9). Any combination of methyl, ethyl, isopropyl, and phenyl groups is tolerated in a substrate library bearing *p*-nitrophenylate as the leaving group. However, PTE shows a marked preference for one stereoisomer over the other. For example, the value of k_{cat}/K_m for the S_P-isomer of ethyl phenyl *p*-nitrophenyl phosphate (Fig. 2, *compound II*) is 100 times larger than the value for the R_P-isomer (Fig. 2, *compound III*) when the Zn^{2+}/Zn^{2+}-substituted enzyme is utilized. Within this modest substrate library, the S_P-isomer is always a better substrate than is the R_P-isomer. The structural determinants to the substrate specificity and stereoselectivity have been assessed by molecular modeling of the more rapidly hydrolyzed S_P-stereoisomer of ethyl phenyl *p*-nitrophenyl phosphate, for

∥ To whom correspondence should be addressed. Tel.: 608-262-4988; Fax: 608-262-1319; E-mail: Hazel_Holden@biochem.wisc.edu.

[1] The abbreviations used are: PTE, phosphotriesterase; CHES, cyclohexylaminoethanesulfonic acid.

example, onto the three-dimensional structure of PTE with bound diethyl 4-methylbenzylphosphonate. If the *p*-nitrophenyl substituent is positioned in the leaving group pocket and the phosphoryl oxygen is placed where it is positioned in the bound inhibitor, then the two remaining substituents are fixed in space within respect to the other two binding regions. With the preferred S_P-isomer, the larger and bulkier substituent is oriented in the same binding pocket as the methylbenzyl group of inhibitor I (Fig. 2), whereas the smaller substituent occupies the same binding pocket as the *pro-R_P* ethoxy group. These binding regions have thus been assigned the names "large pocket," formed by His-257, Leu-271, and Met-317, and "small pocket," formed by Ile-106, Leu-303, and Ser-308. The relative stereochemical relationships between the substrates and inhibitors can be visualized from the structures presented in Fig. 2.

The bacterial phosphotriesterase is a leading candidate for a bioremediation agent that could ultimately be employed for the widespread detoxification of agricultural insecticides and chemical warfare agents. However, the observed stereoselectivity and substrate specificity of the native enzyme dictate that mutant forms of this enzyme with enhanced catalytic properties must be obtained in order to accommodate the structural variations in the toxic compounds already in use. Therefore, structures of PTE complexed with other substrate analogs are essential to more fully quantify those molecular factors that dictate the binding orientations of ligands within the active site. This information is vital for the design of site-directed and combinatorial mutants of PTE. Here, we report the high resolution x-ray crystallographic structures of PTE complexed with diisopropyl methyl phosphonate (Fig. 2, *compound IV*) or triethyl phosphate (Fig. 2, *compound V*).
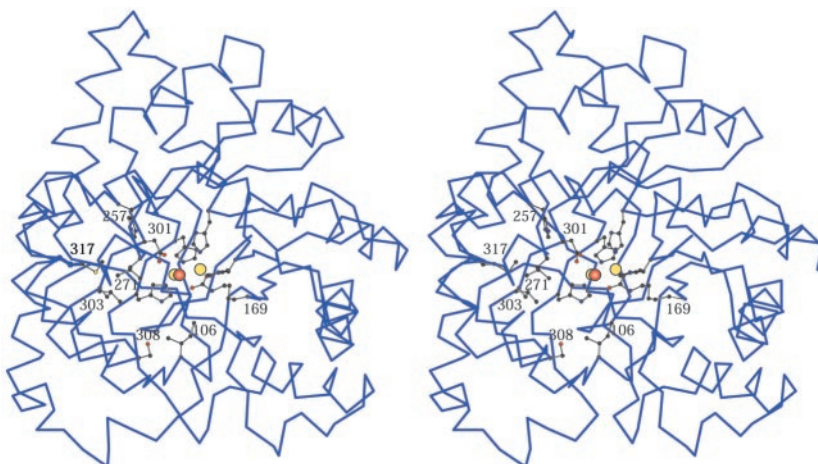
MATERIALS AND METHODS

Protein Purification and Crystallization—The Zn^{2+}/Zn^{2+}-containing enzyme was purified according to a previously published procedure (2). Crystals of the enzyme-diisopropyl methyl phosphonate and the enzyme-triethyl phosphate complexes were grown by macroseeding into small batch setups containing 7% (w/v) polyethylene glycol 8000, 100 mM NaCl, 0.5% (v/v) 2-phenylethanol, 3% (v/v) inhibitor, and 50 mM CHES (pH 9.0) at 4 °C. The protein concentration was typically 5

mg/ml. Crystals of PTE complexed with diisopropyl methyl phosphonate belonged to the space group C2 with unit cell dimensions of $a = 129.4$ Å, $b = 91.0$ Å, $c = 69.2$ Å, and $\beta = 91.6°$ and contained one dimer per asymmetric unit. The Matthews coefficient (10), or V_m, for these crystals was 2.8 Å^3/Da, which corresponds to a solvent content of approximately 56%. Although grown under similar conditions, the crystals of the PTE-triethyl phosphate complex belonged to the space group C222$_1$, with unit cell dimensions of $a = 128.6$ Å, $b = 92.3$ Å, and $c = 69.8$ Å. In this crystal form, there was only one monomer in the asymmetric unit. The V_m for the PTE-triethyl phosphate crystals was also ~2.8 Å^3/Da.

X-ray Data Collection and Processing—X-ray data were collected at 4 °C with a Bruker AXS HiStar area detector system. The x-ray source was nickel-filtered Cu Kα radiation from a Rigaku RU200 x-ray generator operated at 50 mV and 90 mA and equipped with double focusing mirrors. Only one crystal was required to collect each x-ray data set to 1.9 Å resolution. Both x-ray data sets were processed with the software package XDS (11, 12) and internally scaled with the program XCALIBRE.[2] Relevant x-ray data collection statistics are given in Table I.

Structural Determination and Least Squares Refinement—The PTE-diisopropyl methyl phosphonate crystals were isomorphous to those previously employed for the structural analysis of the Zn^{2+}/Zn^{2+}-substituted enzyme complexed with diethyl 4-methylbenzylphosphonate (8). As such, the initial protein phases were calculated on the basis of the refined Zn^{2+}/Zn^{2+}-substituted PTE structure but omitting the inhibitor and the solvent from the x-ray coordinate file. Following several cycles of least squares refinement with the program package TNT (13), the R-factor dropped from 30.9 to 23.0% for all measured x-ray data from 20 to 1.9 Å. Upon inspection of the difference Fourier map, it was clear that the electron densities corresponding to the diisopropyl methyl phosphonates in both subunits were unambiguous. Alternate cycles of manual model building with FRODO (14) and least squares refinement with TNT reduced the R-factor to 18.3% for all measured x-ray data. The final model included 287 water molecules with only one significant

---

[2] G. Wesenberg and I. Rayment, unpublished software.

FIG. 2. **Substrates for phosphotriesterase.** *Compounds II* and *III* are substrates for phosphotriesterase, whereas *compounds I, IV,* and *V* are the inhibitors employed in the structural analysis reported here. *Compound VI* is the chemical warfare agent sarin.

SCHEME 1

FIG. 1. **α-Carbon trace of one subunit of phosphotriesterase.** The overall fold of phosphotriesterase is dominated by eight strands of parallel β-sheet that wrap around to form a barrel that is flanked on the outer surface by α-helices. There are two additional β-strands located at the N terminus that form an antiparallel β-sheet. The active site is located at the C-terminal portion of the β-barrel; the positions of the zinc ions are indicated by the *yellow spheres,* and the side chain ligands are displayed in *ball-and-stick* representations. The metal bound hydroxide is indicated by the *large red sphere.* Those residues defining the small pocket (Ile-106, Leu-303, and Ser-308) and the large pocket (Met-317, Leu-271, and His-257) are labeled.

TABLE I
X-ray data collection statistics

X-ray data set	Resolution	Independent reflections	Completeness	Redundancy	Ave I/Avg σ(I)	R_{sym}[a]
	Å		%			
Diisopropyl methyl phosphonate	1.9	58,525	88.0	2.6	12.4	4.5
Triethyl phosphate	1.9	29,135	92.0	4.3	18.0	4.6

[a] $R_{sym} = (\Sigma \mid I - \mid/\Sigma\ I) \times 100.$

FIG. 3. **Binding pocket for the diisopropyl methyl phosphonate ligand.** Those amino acid residues located within approximately 5.0 Å of the inhibitor are shown. The ligand is highlighted in *yellow bonds*.
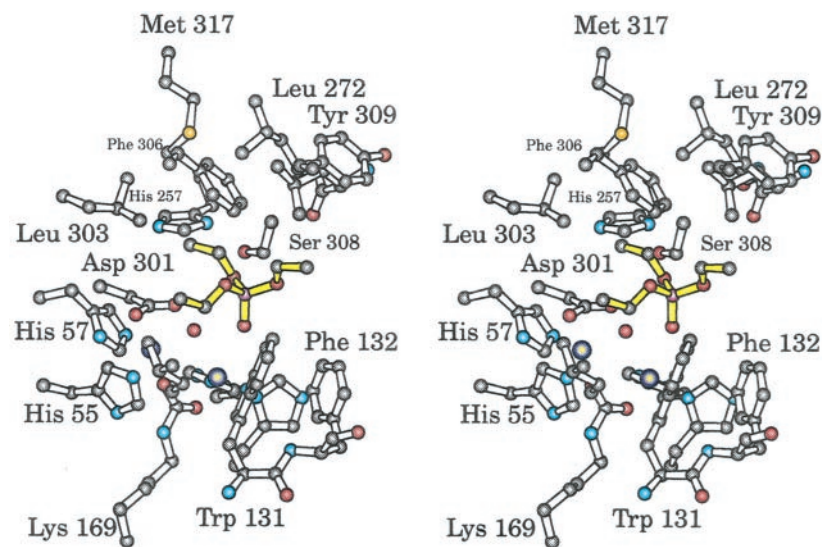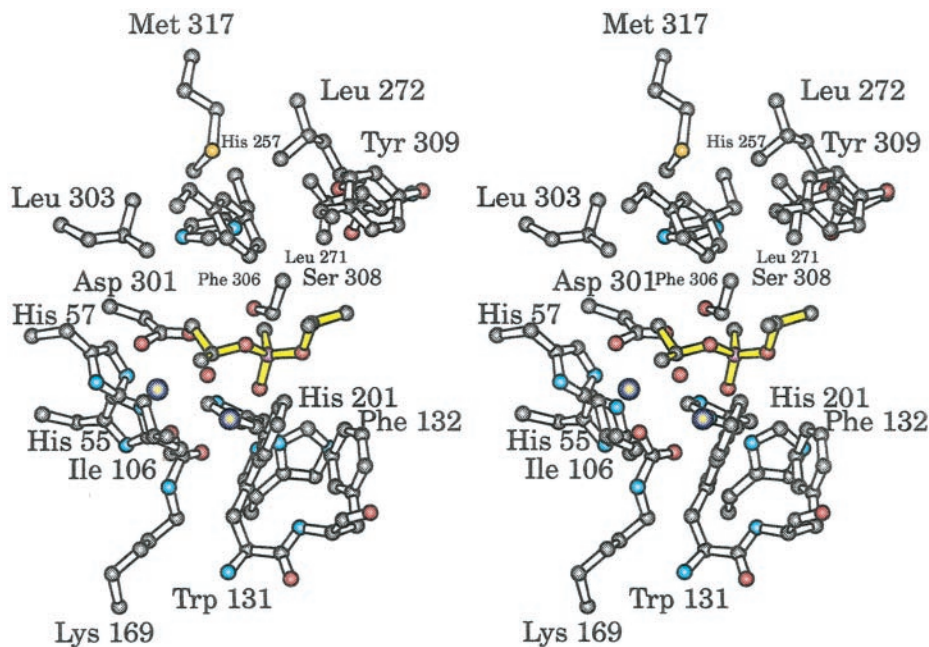

FIG. 4. **Binding pocket for the triethyl phosphate inhibitor.** Those amino acid residues positioned at approximately 5.0 Å of the ligand are included in this stereo representation of the PTE active site. The ligand is highlighted in *yellow bonds*.

outlier per subunit in the Ramachandran plot (Glu-159 with dihedral angles of $\phi = 54.8°$, $\psi = -132.1°$). Refinement statistics are given in Table II.

The PTE-triethyl phosphate structure was determined via molecular replacement with the program AMoRe (15). The Zn^{2+}/Zn^{2+}-substituted enzyme structure was employed as the search model. The rotational and translational solutions resulted in a model with an initial R-factor of 29.3% for all measured x-ray data from 20.0 to 1.9 Å. Like that observed for the PTE-diisopropyl methyl phosphonate complex, the electron density for the triethyl phosphate was well defined. Following the addition of 223 solvent molecules and several rounds of manual model building and least squares refinement, the R-factor dropped to 14.8% for all measured x-ray data. This low R-factor is a reflection of the high quality of both the x-ray data and the refined model. Relevant refinement statistics are presented in Table II. Again the only signifi-

cant outlier in the Ramachandran plot was Glu-159 ($\phi = 53.9°$, $\psi = -132.2°$).

RESULTS AND DISCUSSION

Structure of the PTE-Diisopropyl Methyl Phosphonate Complex—Crystals of PTE complexed with diisopropyl methyl phosphonate belonged to the space group C2 and contained a homodimer in the asymmetric unit. For the two monomers in the asymmetric unit, the average *B*-factors for the protein atoms, the zincs, the solvents, and the inhibitors were 26.8, 15.6, 35.3, and 28.6 Å^2, respectively. In light of the fact that the root mean square deviation between all backbone atoms for the two subunits in the asymmetric unit was 0.14 Å, the following discus-

FIG. 5. **Superposition of the three inhibitors bound in the PTE active site.** The diethyl 4-methylbenzylphosphonate, diisopropyl methyl phosphonate, and triethyl phosphate ligands are shown in *red, blue,* and *green,* respectively.
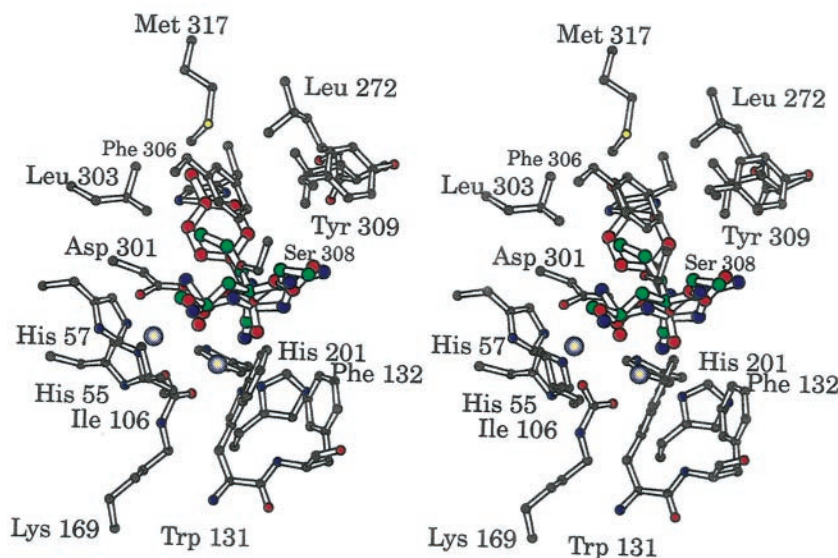
TABLE II
Least squares refinement statistics

	Diisopropyl methyl phosphonate	Triethyl phosphate
Resolution limits (Å)	20.0–1.9	20.0–1.9
R overall (%)[a]	18.3	14.8
R free (%)[b]	24.1	21.1
No. of reflections used	58,525	29,135
No. of protein atoms	5034	2526
No. of solvent atoms[c]	322	243
Weighted root mean square deviations from ideality		
Bond length (Å)	0.012	0.010
Bond angle (°)	2.09	2.10
Planarity (trigonal) (Å)	0.006	0.005
Planarity (other planes) (Å)	0.008	0.007
Torsional Angle (°)[d]	15.8	15.2

[a] R-factor = $(\Sigma|F_o - F_c|/\Sigma|F_o|) \times 100$, where F_o is the observed structure-factor amplitude and F_c is the calculated structure-factor amplitude.

[b] For the required calculation of R free, 10% of the x-ray data were removed from the reflection file.

[c] These include 287 waters, 4 zinc ions, and 2 inhibitor molecules for the PTE/diisopropyl methyl phosphonate model and 223 water, 2 zinc ions, one 2-phenylethanol molecule, and 1 inhibitor molecule for the PTE/triethyl phosphate model.

[d] The torsional angles were not restrained during the refinement.

sion will refer only to the first subunit in the x-ray coordinate file.

Diisopropyl methyl phosphonate was chosen for this study to mimic the binding of the chemical warfare agent sarin to phosphotriesterase (Fig. 2, *compound VI*). The only difference between diisopropyl methyl phosphonate and sarin is replacement of the fluoro leaving group of the nerve agent with an isopropyl group. As can be seen in Fig. 3, one of the isopropyl groups of the ligand faces toward the solvent and abuts the hydrophobic region formed by Trp-131 and Phe-132. Presumably, this is the pocket that accommodates the fluoro group in sarin. The second isopropyl moiety is directed toward His-57, which serves as a ligand to the more buried zinc ion. Finally, the methyl group of the inhibitor points toward His-257 and Leu-271.

The inhibitor binding pocket is characterized by a lack of direct electrostatic interactions between the ligand and the protein. Indeed, only one potential hydrogen bond (3.2 Å) occurs between $N^{\epsilon 1}$ of Trp-131 and the phosphoryl oxygen of the diisopropyl methyl phosphonate. The two zinc ions of phosphotriesterase are separated by 3.3 Å. As previously observed in
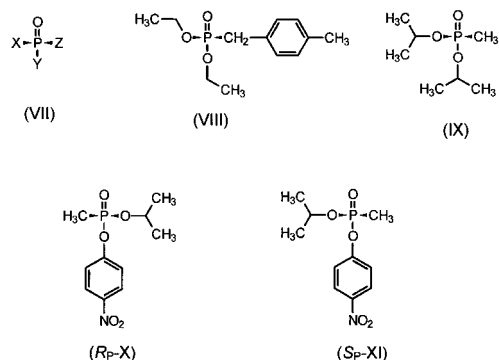

FIG. 6. **Simple representations of organophosphate or organophosphonates.** *Compounds VIII* and *IX* are inhibitors of PTE, whereas *compounds X* and *XI* are substrates.

the PTE-diethyl 4-methylbenzylphosphonate complex (8), the more buried zinc ion is surrounded in a trigonal bipyramidal arrangement by five ligands (His-55, His-57, Asp-301, the carboxylated Lys-169, and a hydroxide ion). In the complex described here, however, the more solvent-exposed metal ion is coordinated by His-201, His-230, the bridging hydroxide, the bridging carboxylated Lys-169, and the phosphoryl oxygen of the inhibitor in a distorted trigonal bipyramidal ligation sphere. This is in contrast to that observed for the PTE-diethyl 4-methylbenzylphosphonate complex whereby the more solvent-exposed metal ion is tetrahedrally coordinated. The ligand:metal ion bond distances for the PTE-diisopropyl methyl phosphonate complex range in length from 1.7 to 2.3 Å, with an average length of 2.1 Å. The distance between the phosphoryl oxygen of the diisopropyl methyl phosphonate and the more solvent-exposed zinc ion is 2.5 Å as opposed to 3.5 Å observed in the previously determined PTE-diethyl 4-methylbenzylphosphonate complex. This shorter distance provides additional support for a catalytic mechanism that involves binding of the substrate phosphoryl oxygen to the more solvent-exposed zinc ion (8, 16).

Structure of the PTE-Triethyl Phosphate Complex—In the case of the PTE-triethyl phosphate complex, the crystals belonged to the space group C222$_1$, with one molecule per asymmetric unit. *B*-factors for the protein, the ligand, the zincs, and the solvents were 19.8, 20.7, 7.8, and 34.6 Å^2, respectively. A close-up view of the binding pocket is displayed in Fig. 4. The three ethoxy arms of the inhibitor experience quite different chemical environments, with one positioned near Trp-131 and

Structure of Phosphotriesterase

Phe-132 and directed toward the solvent, the second lying near His-57, and the third pointing quite closely to Phe-306. Indeed, one of the carbons of the inhibitor lies at approximately 3.4 Å from C$^\zeta$ of Phe-306. Clearly, the orientation of Phe-306 in the phosphotriesterase binding pocket limits the size of substrate substituent that can be accommodated at that position within the active site. Mutation of Phe-306 to an alanine residue results in a significant loss in catalytic activity for nearly all of the substrates tested.[3] Therefore, it appears that this residue is critical for the maintenance of the structural integrity of the active site.

As can be seen in Fig. 4, triethyl phosphate binds within the PTE active site such that its phosphoryl oxygen is positioned at 3.4 Å from the more solvent accessible zinc ion. The two zinc ions are separated by 3.5 Å. As expected, the ligands surrounding the more buried zinc ion adopt a trigonal bipyramidal arrangement (His-55, His-57, Asp-301, the carboxylated Lys-169, and a hydroxide ion) with metal:bond distances ranging in length from 2.0 to 2.2 Å. Unlike the PTE-diisopropyl methyl phosphonate complex, however, in this case, the more solvent-exposed zinc is tetrahedrally ligated by His-201, His-230, the bridging hydroxide, and the carboxylated Lys-169. Note that in this complex, N$^{\epsilon 1}$ of Trp-131 is positioned at 3.6 Å from the phosphoryl oxygen of the substrate analog. With respect to the overall polypeptide chains, the two complexes described here are virtually identical and superimpose with a root mean square deviation of 0.16 Å for all backbone atoms.

Comparison of Inhibitor Binding—Shown in Fig. 5 is a comparison of the mode of binding for the three inhibitors of phosphotriesterase that have been structurally characterized thus far: diethyl 4-methylbenzylphosphonate, diisopropyl methyl phosphonate, and triethyl phosphate. The polypeptide chains for all three protein:inhibitor complexes are virtually identical. Of particular significance is the difference in the positions of the phosphoryl groups of each inhibitor with respect to the move solvent-exposed zinc ion. Within x-ray coordinate error, the phosphoryl group of the diisopropyl methyl phosphonate (or sarin mimic) is significantly closer to the zinc at 2.5 Å than observed for diethyl 4-methylbenzylphosphonate and triethyl phosphate (~3.4 Å) and indeed serves as a ligand to the zinc. Due to the position of Phe-306, the 4-methylbenzyl moiety of the diethyl 4-methylbenzylphosphonate is pushed back, relative to that observed for the triethyl phosphate ligand, into the large binding pocket. From Fig. 5, it is clear that the PTE binding pocket is quite large, which explains, in structural terms, the wide range of substrates that can be hydrolyzed by this unique enzyme.

Shown in Fig. 6 is a simple representation of an organophosphate or organophosphonate complex (VII) bearing three substituents labeled *X, Y,* and *Z*. Within the active site of PTE, substituents X, Y, and Z would be bound within the small, leaving group, and large subsites, respectively. If we orient the two prochiral substrate analogs in the manner in which they are bound to the active site of PTE, then the relative orientations of the three substituents are as indicated in structures VIII and IX for diethyl 4-methylbenzylphosphonate and diiso-

propyl methyl phosphonate, respectively. With these two substrate analogs, the lone phosphonate substituent could have been found in any one of three different orientations by occupying either the small, large, or leaving group subsites. However, the x-ray structural data clearly indicate that one of the three possible orientations within the active site of PTE is greatly preferred over the other two. The observed orientation must be the more thermodynamically stable conformation within the crystalline lattice. It is interesting to note that the two phosphonate substituents (methyl and methylbenzyl) are each orientated within the large subsite, even though these two substituents are of different relative sizes, compared with the other two substituents within the same molecule. Therefore, the factors that dictate the positioning of these moieties in the active site of PTE are not based entirely on the relative physical bulk of the substituents themselves. Moreover, the relative positioning of these two substrate analogs within the active site of PTE does not correlate with the expectations based on the observed stereoselectivity for chiral substrates of very similar structure. For example, Co^{+2}/Co^{+2}-PTE has been shown to prefer the R_P-enantiomer of isopropyl *p*-nitrophenyl methyl phosphonate (X) over the S_P-enantiomer (XI) by a factor of about 20.[4] Thus, for the preferred R_P-isomer (X), the methyl and *O*-isopropyl substituents must be bound to the small and large subsites during productive catalytic turnover. However, this is the opposite placement of these two substituents in the bound complex of diisopropyl methyl phosphonate (IX). This observation suggests that nonproductive complexes are readily formed during the binding and subsequent catalytic turnover of substrates by PTE, and as such, one must proceed with caution when using x-ray structural data alone in the redesign of enzyme active sites for the modification of their catalytic properties.

REFERENCES

1. Caldwell, S. R., and Raushel, F. M. (1991) *Appl. Biochem. Biotechnol.* **31,** 59–73
2. Omburo, G. A., Kuo, J. M., Mullins, L. S., and Raushel, F. M. (1992) *J. Biol. Chem.* **267,** 13278–13283
3. Raushel, F. M., and Holden, H. M. (2000) *Adv. Enzymol.* **74,** 51–93
4. Benning, M. M., Kuo, J. M., Raushel, F. M., and Holden, H. M. (1994) *Biochemistry* **33,** 15001–15007
5. Benning, M. M., Kuo, J. M., Raushel, F. M., and Holden, H. M. (1995) *Biochemistry* **34,** 7973–7978
6. Jabri, E., Carr, M. B., Hausinger, R. P., and Karplus, P. A. (1995) *Science* **268,** 998–1004
7. Wilson, D. K., Rudolph, F. B., and Quiocho, F. A. (1991) *Science* **252,** 1278–1284
8. Vanhooke, J. L., Benning, M. M., Raushel, F. M., and Holden, H. M. (1996) *Biochemistry* **35,** 6020–6025
9. Hong, S.-B., and Raushel, F. M. (1999) *Biochemistry* **38,** 1159–1165
10. Matthews, B. W. (1968) *J. Mol. Biol.* **33,** 491–497
11. Kabsch, W. (1988) *J. Appl. Crystallogr.* **21,** 67–71
12. Kabsch, W. (1988) *J. Appl. Crystallogr.* **21,** 916–924
13. Tronrud, D. E., Ten Eyck, L. F., and Matthews, B. W. (1987) *Acta Crystallogr. Sect. A* **43,** 489–501
14. Jones, T. A. (1985) *Methods Enzymol.* **115,** 157–171
15. Navaza, J. (1994) *Acta Crystallogr. Sect. A* **50,** 157–163
16. Hong, S.-B., and Raushel, F. M. (1996) *Biochemistry* **35,** 10904–10912

[3] M. Chen-Goodspeed and M. Sogorb, unpublished results.

[4] M. Chen-Goodspeed, unpublished data.